

Spectroscopic analysis of southern B and Be stars

R. S. Levenhagen¹* and N. V. Leister¹†

¹*Instituto de Astronomia, Geofísica e Ciências Atmosféricas da Universidade de São Paulo, CUASO 05508-900 São Paulo, Brazil*

Accepted 1988 December 15. Received 1988 December 14; in original form 1988 October 11

ABSTRACT

Spectroscopic monitoring of 141 southern field B type stars, 114 of them known to exhibit the Be phenomenon, allowed the estimation of their projected rotational velocities, effective temperatures and superficial gravities from both line and equivalent width fitting procedures. Stellar ages, masses and bolometric luminosities were derived from internal structure models. Without taking into account for the effects of gravity darkening, we notice the occurrence of the Be phenomenon in later stages of main sequence phase.

Key words: line: profile – stars: emission-line – stars: fundamental parameters – stars: rotation – techniques: spectroscopic.

1 INTRODUCTION

Despite the large amount of works on the subject of B and Be stars published in the past years, both theoretical and observational, there are still many remaining unsolved problems concerning their outstanding peculiarities. Among them the origin of their high rotation velocities, dependence of Be frequency counts with evolutionary stages in the main sequence, presence and origin of magnetic fields and mass loss (Vinicius et al. 2006, McSwain & Gies 2005, Levenhagen & Leister 2004, Levenhagen et al 2003, Porter & Rivinius 2003).

Concerning particularly the case of Be stars, the most outstanding observable characteristic in the visible domain is the existence of emission in Balmer lines, being often accompanied by emission of singly ionized metals and changes of the spectrophotometric characteristics (Moujtahid et al. 1999; Levenhagen 2004). In these stars, emissions and energy distributions are variable and the most important among these variations are “phase transitions”, which most likely reflect changes in the structure of the circumstellar envelope (CE) and processes related with its formation.

One of the fundamental questions related to the Be phenomenon concerns the origin of the fast rotation rates of the central star. Rotation has quite different effects on stellar evolution, as changes of internal hydrostatic equilibrium, transport of chemical species by meridional circulation and effects on mass loss rates (Maeder 1999).

These days it is a consense that fast surface rotation plays a crucial role in triggering the Be phenomenon, where

the onset of new observational evidences indicate that these objects are in fact near critical rotators, with $\omega \simeq 0.88$ (Zorec, Frémat & Cidale 2005, Frémat et al. 2005, Townsend, Owocki & Howarth 2004).

There are actually three main possibilities for that: (i) it would be a permanent innate property; (ii) it would be due to spin up by binary mass transfer; (iii) or it would be acquired somehow during the main sequence evolution phase (Crampin & Hoyle 1960, Schild & Romanishin 1976). Early attempts to describe the Be phenomenon suggested the occurrence of Be stars during the secondary contraction phase (Schmidt-Kaler 1964). A few years later, it was seen the appearance of a significant fraction of Be stars close to the ZAMS (Schild & Romanishin 1976). In the 80's it was generally accepted that those objects occupy the whole main sequence band at different evolutionary phases (Mermilliod 1982; Slettebak 1985).

Maeder, Grebel & Mermilliod (1999) explained the origin of high rotation rates by two possible scenarios of low metallicity effects in star formation regions. In the first scenario a weak coupling of magnetic fields with star forming matter leads to less angular momentum losses and a consequent spin-up. The second possibility is based on a low opacity effect in the pre main sequence phase which in turn determines the external convective zones to fade away and thus leading to less angular momentum losses.

Today some works present the Be phenomenon as a result of an evolutionary effect instead (Fabregat & Torrejón 2000). In a recent work on Be stars in open clusters, McSwain & Gies (2005) pointed out that the Be phenomenon is not strongly dependent on metallicity or cluster density, instead it is influenced by the evolutionary stage. One problem with those studies is that they rely on photometric measurements only, which tends, in the case of Be stars, to sys-

* E-mail: savarino@astro.iag.usp.br (RSL)

† This study is based on observations made at ESO La Silla, Chile and MCT/LNA, Brazil.

tematically overestimate the magnitudes due to the presence of a circumstellar environment. On the other hand, Zorec et al (2006) determined photospheric parameters of a sample of 97 field Be stars near the Sun based on spectroscopic measurements considering both rotating and non-rotating model atmosphere scenarios. In this work they found that, without taking into account for the effects of fast rotation in the models, Be stars usually appear near the TAMS rather than the ZAMS in the HR diagram, i.e. the Be phenomenon would arise due to an apparent evolutionary effect. Later on, considering the effects of gravity darkening, the stellar distribution in the HR diagram becomes more homogeneous, and Be stars are allowed to occur at any stages within the main sequence phase. In order to elucidate this problem further investigations are still needed.

In this paper we present the results of spectroscopic analyses carried out with 141 southern B stars (where 114 are field Be stars), some of them located away from the solar neighbourhood, in order to provide physical parameters estimations of $V\sin i$, T_{eff} and $\log g$, and interpolations in the tabulated evolutionary tracks by Schaller et al. (1992) necessary for further investigations on these objects. These parameters have been estimated from NLTE model atmospheres without taking into account for gravitational darkening (von Zeipel 1924a,b) and their positions in the HR diagram were established. We also estimated the errors committed in the physical parameters ($T_{\text{eff}}, \log g$) by neglecting the rotational effects.

2 OBSERVATIONS

High resolution and signal-to-noise spectroscopic observations were carried out in the Southern Hemisphere both with FEROS spectrograph associated to the 1.52m telescope at ESO/La Silla (Chile) and with Coudé spectrograph at the 1.60m telescope of MCT/LNA (Brazil). We made observations of B and Be stars over 5 years, from October/1999 to July/2003. ESO spectra were taken with a spectral coverage of 3560-9200 Å, with typical $S/N \sim 200$ and a reciprocal dispersion of 0.09 Å/pixel, concerning the He I 4471 Å line. LNA spectra were gathered with two CCD cameras: a WI101 CCD from 4279 Å to 4720 Å with reciprocal dispersion of 0.43 Å/pixel (at 4471 Å) and a WI098 CCD from 3939 Å to 5060 Å with a reciprocal dispersion of 0.24 Å/pixel (at 4471 Å) using a 600 groove mm⁻¹ grating blazed at 4500 Å in first order and typical S/N ratio ~ 150 (For more details see Table 1). The images were processed in the same sense, basically starting with bias and overscan subtraction, followed by the division of the stellar spectra by an average flat-field exposure, compiled from all the flat fields taken during the night. The spectra were then wavelength-calibrated and corrected for telluric line contamination. Standard stars of rotation velocity and flux were also observed. All the mentioned data reduction was accomplished using the IRAF¹ package.

¹ IRAF is distributed by the National Optical Astronomy Observatories, which is operated by the Association of Universities for Research in Astronomy (AURA), Inc., under cooperative agreement with the National Science Foundation

2.1 Spectroscopic analysis and results

In this work we derive the ($T_{\text{eff}}, \log g$) parameters with the use of non-LTE model atmospheres neglecting the effects of gravity darkening on the shape of line profiles. As Be stars are fast rotators, these photospheric quantities actually reflect only the average apparent photospheric characteristics, ie. those of the observed stellar hemisphere deformed by the fast rotation (Frémat et al. 2005).

The determination of stellar temperatures, gravities and rotation velocities is achieved in this work in basically three steps:

(i) First guess of $V\sin i$ from the average of Fourier Transforms (FT) of all neutral helium lines in the domain 4000 to 5000 Å. To this end we adopted a quadratic limb-darkening law (Wade & Rucinski 1985) to determine the rotational broadening function (Gray 1992; Carroll 1933) of the form:

$$G(y) = C_1(1 - y^2)^{1/2} + C_2(1 - y^2) + C_3(1 - y^2)^2 \quad (1)$$

where C_1 , C_2 and C_3 are constants dependent on the linear and quadratic limb-darkening coefficients. The Fourier Transform of the broadening function can be written as:

$$\begin{aligned} g(\alpha) &= 2 \int_0^1 G(y) \cos \sigma b y dy = \\ &= C_1 \pi \frac{J_1(\alpha)}{\alpha} \left(1 + \frac{6}{\alpha^2} \frac{C_3}{C_1} \right) + \\ &+ C_2 \left(\frac{2}{\alpha} \right)^2 \left(\frac{\sin \alpha}{\alpha} - \cos \alpha \right) - 3\pi C_3 \frac{J_0(\alpha)}{\alpha^2} \end{aligned} \quad (2)$$

The rotation velocity values are then estimated from the ratio of the first zero of the broadening function's TF (α_1) and the first zero of the TF of the observed profile (ν_1) as:

$$V\sin i = \frac{c}{\lambda_0} \frac{\alpha_1}{2\pi\nu_1} \quad (3)$$

This method is suitable only for a first guess on $V\sin i$ values (Levenhagen 2004, Levenhagen & Leister 2004), but takes into account only for limb-darkening coefficients related to the continuum spectrum and the effect of gravity darkening is not considered;

(ii) First estimation of effective temperature and superficial gravity through the ionization equilibria of He II/He I, Si III/Si II, O III/O II, N III/N II and Balmer equivalent width fitting, constraining the initial solutions to some determined region in the ($T_{\text{eff}}, \log g$) plane. For this sake it were used LTE atmosphere models from Kurucz (1992). This process originates a series of curves in the ($T_{\text{eff}}, \log g$) plane which intercept each other delimiting regions of possible solutions where the best one is to be given by its baricentre. In order to choose which region is well suitable to a given object we compare each baricentre value with ($T_{\text{eff}}, \log g$) values determined from photometric Johnson's UBV, Strömgren uvby and H β values for that specific object in the literature, and taking into account its spectral classification. In the particular case of Be stars, the presence of circumstellar environment (CE) emission causes an overestimation of m_v magnitudes. An attempt to clear up this effect was to employ the corrections proposed by Zorec & Briot (1997) for each subspectral type;

(iii) Once established a first guess of ($T_{\text{eff}}, \log g$,

Table 1. Spectroscopic observations of target objects.

Object	ℓ (o)	b (o)	α (J2000)	δ (J2000)	Telescope	Epoch	Wavelength range (Å)
HD 10144	290.84	-58.79	1 37 42	-57 14 12	ESO 1.52 m	October/1999	3560 - 9200
HD 14850	225.38	-69.74	2 23 0	-29 37 10	ESO 1.52 m	October/2001	3560 - 9200
HD 15371	267.12	-62.24	2 26 59	-47 42 13	LNA 1.60 m	July/2003	3939 - 5060
HD 16582	170.76	-52.21	2 39 28	0 19 42	LNA 1.60 m	July/2003	3939 - 5060
HD 17891	143.59	-10.73	02 54 00	47 09 39	ESO 1.52 m	October/2001	3560 - 9200
HD 20340	203.36	-55.13	03 15 45	-16 49 43	ESO 1.52 m	October/2001	3560 - 9200
HD 28248	267.15	-42.23	4 24 6	-57 15 11	ESO 1.52 m	September/2002	3560 - 9200
HD 29557	223.65	-39.36	4 38 16	-24 39 30	ESO 1.52 m	October/2001	3560 - 9200
HD 33453	245.40	-36.21	5 8 26	-40 54 44	ESO 1.52 m	October/2001	3560 - 9200
HD 33599	271.32	-35.91	5 7 12	-61 48 18	ESO 1.52 m	October/2001	3560 - 9200
HD 35165	238.07	-32.61	5 21 16	-34 20 42	ESO 1.52 m	October/2001	3560 - 9200
HD 35468	196.93	-15.95	5 25 7	6 20 58	ESO 1.52 m	September/2002	3560 - 9200
HD 36012	201.19	-17.25	5 28 48	2 9 52	ESO 1.52 m	October/2001	3560 - 9200
HD 36861	195.05	-11.99	5 35 8	9 56 5	ESO 1.52 m	September/2002	3560 - 9200
HD 37023	209.01	-19.38	5 35 17	-5 23 15	ESO 1.52 m	September/2002	3560 - 9200
HD 37490	200.73	-14.03	5 39 11	4 07 17	ESO 1.52 m	April/2001	3560 - 9200
HD 37795	238.81	-28.86	5 39 38	-34 4 26	ESO 1.52 m	October/2001	3560 - 9200
HD 37935	276.51	-32.10	5 36 55	-66 33 37	ESO 1.52 m	October/2001	3560 - 9200
HD 43122	244.10	-23.20	6 12 49	-37 4 53	ESO 1.52 m	October/2001	3560 - 9200
HD 43285	203.42	-5.13	6 15 40	6 3 58	ESO 1.52 m	October/2001	3560 - 9200
HD 43544	224.13	-15.15	06 16 07	-16 37 04	ESO 1.52 m	October/2001	3560 - 9200
HD 43789	252.20	-24.71	06 15 56	-44 37 10	ESO 1.52 m	October/2001	3560 - 9200
HD 44743	226.06	-14.27	06 22 41	-17 57 21	ESO 1.52 m	October/2001	3560 - 9200
HD 44996	221.58	-11.80	06 24 20	-12 57 42	ESO 1.52 m	October/2001	3560 - 9200
HD 45871	240.47	-18.59	06 28 39	-32 22 16	ESO 1.52 m	October/2001	3560 - 9200
HD 46131	230.96	-14.35	06 30 38	-22 19 18	ESO 1.52 m	October/2001	3560 - 9200
HD 46380	217.53	-7.56	06 32 43	-07 30 32	ESO 1.52 m	October/2001	3560 - 9200
HD 47839	202.94	+2.20	06 40 58	+09 53 44	ESO 1.52 m	October/2001	3560 - 9200
HD 48099	206.21	+0.80	06 41 59	+06 20 43	ESO 1.52 m	October/2001	3560 - 9200
HD 48282	221.28	-6.79	06 42 12	-10 29 53	ESO 1.52 m	October/2001	3560 - 9200
HD 49131	240.50	-14.73	06 45 31	-30 56 56	ESO 1.52 m	October/2001	3560 - 9200
HD 49319	248.84	-17.84	06 46 03	-39 32 24	ESO 1.52 m	October/2001	3560 - 9200
HD 49320	211.84	-0.42	06 47 57	+00 46 34	ESO 1.52 m	October/2001	3560 - 9200
HD 49336	247.13	-17.18	06 46 12	-37 46 31	ESO 1.52 m	October/2001	3560 - 9200
HD 50013	242.36	-14.49	06 49 50	-32 30 30	ESO 1.52 m	April/2000	3560 - 9200
HD 50209	213.28	+0.03	06 52 10	-00 17 43	ESO 1.52 m	October/2001	3560 - 9200
HD 50696	213.10	+0.74	06 54 22	+00 10 54	ESO 1.52 m	October/2001	3560 - 9200
HD 50737	224.98	-5.44	06 53 52	-13 11 09	ESO 1.52 m	October/2001	3560 - 9200
HD 50850	229.61	-7.65	06 54 09	-18 17 10	ESO 1.52 m	October/2001	3560 - 9200
HD 51309	228.70	-6.68	06 56 08	-17 03 15	ESO 1.52 m	October/2001	3560 - 9200
HD 52159	223.81	-3.25	06 59 42	-11 09 26	ESO 1.52 m	October/2001	3560 - 9200
HD 52244	228.33	-5.52	06 59 46	-16 12 02	ESO 1.52 m	October/2001	3560 - 9200
HD 55606	217.31	+3.97	07 13 34	-02 04 39	ESO 1.52 m	October/2001	3560 - 9200
HD 58715	209.52	+11.68	07 27 09	+08 17 21	LNA 1.60 m	May/2001	4279 - 4720
HD 59868	257.26	-12.53	07 29 48	-44 54 42	ESO 1.52 m	October/2001	3560 - 9200
HD 63150	251.17	-5.90	07 45 55	-36 29 53	LNA 1.60 m	May/2001	4279 - 4720
HD 67698	242.66	+4.92	08 08 19	-23 37 04	ESO 1.52 m	April/2001	3560 - 9200
HD 70461	246.56	+5.87	08 21 13	-26 19 59	ESO 1.52 m	April/2001	3560 - 9200
HD 74280	223.25	+26.32	08 43 13	+03 23 55	LNA 1.60 m	May/2001	4279 - 4720
HD 79447	280.22	-9.61	09 11 16	-62 19 01	LNA 1.60 m	May/2001	4279 - 4720
HD 90177	285.15	-1.98	10 22 53	-59 37 28	LNA 1.60 m	May/2003	3939 - 5060
HD 100546	296.37	-8.32	11 33 25	-70 11 41	LNA 1.60 m	June/2003	3939 - 5060
HD 100889	274.25	48.86	11 36 40	-9 48 8	LNA 1.60 m	May/2001	3939 - 5060
HD 104582	296.73	2.95	12 2 35	-59 20 13	ESO 1.52 m	August/2001	3560 - 9200
HD 105435	296.00	11.57	12 8 21	-50 43 20	LNA 1.60 m	May/2003	3939 - 5060
HD 105521	294.39	20.93	12 8 54	-41 13 53	LNA 1.60 m	July/2003	3939 - 5060
HD 105937	296.78	10.03	12 11 39	-52 22 6	LNA 1.60 m	February/2003	3939 - 5060
HD 106309	298.18	3.13	12 14 01	-59 23 48	LNA 1.60 m	May/2001	4279 - 4720
HD 106793	298.15	6.14	12 16 59	-56 24 24	LNA 1.60 m	May/2001	4279 - 4720
HD 110432	301.96	-0.20	12 42 50	-63 3 31	LNA 1.60 m	July/2003	3939 - 5060
HD 110699	302.05	3.72	12 44 37	-59 9 36	ESO 1.52 m	August/2001	3560 - 9200
HD 112078	303.35	3.72	12 54 39	-59 8 48	LNA 1.60 m	July/2003	3939 - 5060
HD 112091	303.37	5.70	12 54 36	-57 10 7	LNA 1.60 m	July/2003	3939 - 5060
HD 112107	303.44	10.38	12 54 41	-52 29 2	ESO 1.52 m	April/2001	3560 - 9200
HD 112512	303.78	3.78	12 58 00	-59 05 03	LNA 1.60 m	May/2001	4279 - 4720
HD 113120	303.87	-8.63	13 3 5	-71 28 32	LNA 1.60 m	July/2003	3939 - 5060
HD 118094	307.98	-0.71	13 36 20	-63 8 44	LNA 1.60 m	July/2003	3939 - 5060
HD 119423	308.22	-4.44	13 45 18	-66 45 16	ESO 1.52 m	July/2002	3560 - 9200
HD 119682	309.16	-0.72	13 46 32	-62 55 24.13	ESO 1.52 m	July/2002	3560 - 9200
HD 120324	314.24	19.12	13 49 36	-42 28 25	LNA 1.60 m	July/2003	3939 - 5060

$V \sin i$) parameters, we continue with a more detailed line fitting procedure with theoretical profiles synthesized with the SYNSPEC fortran program (Hubeny, Hummer, & Lanz 1994) in the spectral range 4000 to 5000 Å from a grid of non-LTE stellar atmosphere models generated with TLUSTY code (Hubeny 1988). The fitting procedure is performed with models calculated for a parameter space around the starting ($T_{\text{eff}}, \log g, V \sin i$) set using the downhill simplex algorithm (Nelder & Mead 1965). Figure 1 shows the fittings of He I 4471 Å and Mg II 4481 Å line profiles for 8 sample stars. The same fitting procedure was adopted for all 141 B/Be objects. In Figure 2 we show more detailed fittings achieved to the observed spectrum of Achernar (HD 10144) in wavelength regions near the Balmer ($H\beta$, $H\gamma$, $H\delta$) lines. In some observed slow rotating Be stars where $V \sin i \lesssim 100$ km s⁻¹, which are probably seen pole-on, the emission in the $H\gamma$ line profile is often present. This emission makes uncer-

tain the line fitting procedure with models. In such cases we used the method outlined in Chauville et al. (2001). Choosing two points x_1 and x_2 in the spectrum (with $x_i = \lambda_i - \lambda_c$), a third point is given by:

$$x_3 = (x_1 x_2)^{1/2} \quad (4)$$

By definition the ordinate values related to x_1 , x_2 and x_3 are given through:

$$y_i = -[\ln \psi^{\text{obs}}(\lambda_i)]^{-1} \quad (5)$$

where ψ^{obs} is the observed profile. The final adjusted profile $\psi(\lambda)$ is of the form:

$$\psi(\lambda) = \exp \left\{ -[a(\lambda - \lambda_c)^b + c]^{-1} \right\} \quad (6)$$

where the constants a , b and c are related by:

Table 1. Continued.

Object	ℓ (o)	b (o)	α (J2000)	δ (J2000)	Telescope	Epoch	Wavelength range (Å)
HD 120991	313.84	14.42	13 53 57	-47 7 41	LNA 1.60 m	May/2001	4279 - 4720
HD 124639	305.94	-20.53	14 24 22	-82 50 53	ESO 1.52 m	July/2002	3560 - 9200
HD 126527	316.38	4.86	14 27 56	-55 28 10	ESO 1.52 m	August/2001	3560 - 9200
HD 126986	317.93	7.71	14 30 32	-52 15 20	ESO 1.52 m	August/2001	3560 - 9200
HD 127112	315.59	1.49	14 31 45	-58 53 22	ESO 1.52 m	August/2001	3560 - 9200
HD 127208	331.15	34.91	14 30 40	-22 27 39	ESO 1.52 m	April/2001	3560 - 9200
HD 127381	318.93	9.25	14 32 37	-50 27 25	LNA 1.60 m	May/2001	4279 - 4720
HD 127972	322.77	16.67	14 35 30	-42 9 28	ESO 1.52 m	April/2000	3560 - 9200
HD 129956	353.72	51.97	14 45 30	0 43 2	LNA 1.60 m	May/2001	4279 - 4720
HD 130437	317.22	-0.77	14 50 50	-60 17 10	ESO 1.52 m	April/2000	3560 - 9200
HD 130534	320.76	6.43	14 50 41	-52 15 52	ESO 1.52 m	August/2001	3560 - 9200
HD 131168	324.10	11.94	14 53 22	-45 51 20	ESO 1.52 m	April/2001	3560 - 9200
HD 132947	317.37	-4.06	15 4 56	-63 7 52	ESO 1.52 m	April/2000	3560 - 9200
HD 134401	316.69	-6.96	15 13 12	-65 58 9	ESO 1.52 m	August/2001	3560 - 9200
HD 134481	325.46	7.89	15 11 56	-48 44 16	LNA 1.60 m	July/2003	3939 - 5060
HD 134671	324.57	6.09	15 13 2	-50 44 6	ESO 1.52 m	April/2001	3560 - 9200
HD 135734	326.86	8.05	15 18 32	-47 52 30	LNA 1.60 m	July/2003	3939 - 5060
HD 136968	324.60	2.47	15 25 55	-53 46 15	LNA 1.60 m	May/2001	4279 - 4720
HD 137387	313.85	-14.01	15 31 30	-73 23 22	LNA 1.60 m	July/2003	3939 - 5060
HD 137518	329.81	9.40	15 28 17	-45 8 5	ESO 1.52 m	April/2001	3560 - 9200
HD 142237	327.41	-1.11	15 56 5	-54 57 9	ESO 1.52 m	April/2001	3560 - 9200
HD 142349	325.82	-3.21	15 57 7	-57 34 48	ESO 1.52 m	August/2001	3560 - 9200
HD 143545	332.29	2.91	16 3 9	-48 43 21	ESO 1.52 m	August/2001	3560 - 9200
HD 143578	341.31	13.00	16 2 38	-35 15 11	ESO 1.52 m	April/2001	3560 - 9200
HD 143700	333.23	3.74	16 4 2	-47 28 33	ESO 1.52 m	August/2001	3560 - 9200
HD 144555	330.81	-0.12	16 8 55	-51 57 43	ESO 1.52 m	August/2001	3560 - 9200
HD 146531	327.66	-5.69	16 19 55	-58 10 1	ESO 1.52 m	August/2001	3560 - 9200
HD 149757	6.28	23.59	16 37 9	-10 34 1	ESO 1.52 m	April/2000	3560 - 9200
HD 150193	355.60	14.83	16 40 17	-23 53 45	ESO 1.52 m	April/2000	3560 - 9200
HD 150288	338.13	-0.54	16 42 16	-47 0 56	ESO 1.52 m	August/2001	3560 - 9200
HD 150422	338.61	-0.31	16 43 7	-46 30 23	ESO 1.52 m	August/2001	3560 - 9200
HD 151113	339.90	-0.21	16 47 30	-45 27 37	ESO 1.52 m	August/2001	3560 - 9200
HD 152060	343.65	1.62	16 52 59	-41 24 27	ESO 1.52 m	September/2001	3560 - 9200
HD 152478	336.78	-4.64	16 56 8	-50 40 29	ESO 1.52 m	August/2001	3560 - 9200
HD 152979	340.64	-2.18	16 58 56	-46 7 44	ESO 1.52 m	August/2001	3560 - 9200
HD 153199	343.04	-0.52	16 59 56	-43 13 14	ESO 1.52 m	April/2001	3560 - 9200
HD 154154	339.57	-4.54	17 6 7	-48 25 7	ESO 1.52 m	August/2001	3560 - 9200
HD 155851	353.32	3.33	17 15 33	-32 41 23	ESO 1.52 m	April/2001	3560 - 9200
HD 156325	353.77	2.93	17 18 20	-32 33 11	ESO 1.52 m	April/2001	3560 - 9200
HD 156702	349.05	-0.98	17 20 50	-38 39 8	ESO 1.52 m	July/2002	3560 - 9200
HD 158427	340.76	-8.83	17 31 50	-49 52 34	ESO 1.52 m	April/2000	3560 - 9200
HD 159489	345.28	-7.10	17 37 13	-45 9 26	ESO 1.52 m	August/2001	3560 - 9200
HD 160202	356.59	-0.69	17 40 1	-32 12 3	ESO 1.52 m	April/2001	3560 - 9200
HD 161774	356.14	-3.14	17 48 51	-33 51 45	LNA 1.60 m	May/2001	4279 - 4720
HD 164284	30.99	13.37	18 0 15	4 22 7	LNA 1.60 m	July/2003	3939 - 5060
HD 164816	6.06	-1.20	18 3 56	-24 18 45	LNA 1.60 m	June/2003	3939 - 5060
HD 164906	6.05	-1.33	18 4 25	-24 23 8	ESO 1.52 m	July/2002	3560 - 9200
HD 164947	6.11	-1.36	18 4 41	-24 20 54	LNA 1.60 m	June/2003	3939 - 5060
HD 165052	6.12	-1.48	18 5 10	-24 23 54	ESO 1.52 m	October/2001	3560 - 9200
HD 166566	14.51	1.38	18 11 50	-15 40 47	ESO 1.52 m	September/2002	3560 - 9200
HD 170235	7.95	-6.73	18 29 21	-25 15 23	ESO 1.52 m	August/2001	3560 - 9200
HD 170835	13.67	-4.58	18 32 16	-19 13 1	ESO 1.52 m	August/2001	3560 - 9200
HD 171054	18.49	-2.34	18 33 8	-13 54 43	ESO 1.52 m	September/2002	3560 - 9200
HD 171219	35.73	6.51	18 33 17	5 26 43	ESO 1.52 m	July/2002	3560 - 9200
HD 172256	11.40	-7.78	18 40 11	-22 39 49	ESO 1.52 m	August/2001	3560 - 9200
HD 173948	333.61	-23.87	18 52 13	-62 11 15	LNA 1.60 m	July/2003	3939 - 5060
HD 174513	25.95	-3.49	18 51 9	-7 47 55	ESO 1.52 m	July/2002	3560 - 9200
HD 174705	22.64	-5.46	18 52 16	-11 37 57	LNA 1.60 m	May/2001	4279 - 4720
HD 179253	355.25	-21.80	19 13 44	-42 24 48	ESO 1.52 m	April/2001	3560 - 9200
HD 183914	62.12	4.57	19 30 45	27 57 54	LNA 1.60 m	July/2003	3939 - 5060
HD 184279	41.15	-7.62	19 33 36	3 45 40	ESO 1.52 m	July/2002	3560 - 9200
HD 185037	70.58	7.89	19 35 48	36 56 40	LNA 1.60 m	July/2003	3939 - 5060
HD 198001	37.68	-30.10	20 47 40	-9 29 44	LNA 1.60 m	May/2001	4279 - 4720
HD 205637	31.94	-44.99	21 37 04	-19 27 57	LNA 1.60 m	July/2003	3939 - 5060
HD 208886	15.64	-52.59	21 59 55	-31 31 32	LNA 1.60 m	May/2001	4279 - 4720
HD 217891	78.79	-49.61	23 3 52	3 49 12	LNA 1.60 m	July/2003	3939 - 5060
HD 224686	311.30	-50.71	23 59 54	-65 34 37	LNA 1.60 m	July/2003	3939 - 5060
HD 316341	359.46	-1.08	17 48 35	-29 57 28	ESO 1.52 m	April/2001	3560 - 9200
HD 316587	359.89	-1.75	17 52 13	-29 55 52	ESO 1.52 m	April/2001	3560 - 9200
HD 322422	344.99	1.63	16 57 23	-40 21 39	ESO 1.52 m	August/2001	3560 - 9200
HD 330950	335.40	-1.30	16 34 43	-49 33 9	ESO 1.52 m	September/2002	3560 - 9200

$$\begin{cases} c = \frac{(y_1 y_2 - y_3^2)}{(y_1 + y_2 - 2y_3)} \\ \ln(y_i - c) = b \ln x_i + a \end{cases} \quad (7)$$

Relation (6) is used to determine the absorption-like underlying photospheric component of the Balmer line seen in emission, or in the worst cases where the star is in full emission we estimated the T_{eff} and $\log g$ parameters using only the $H\delta$ profile.

To perform the operation outlined in step (ii) we use, whenever possible, lines in two neighbouring ionization states since their equivalent width ratios are less sensitive to the abundance of elements. For cooler stars however, it is conspicuous the occurrence of neutral helium lines, since strong He II lines in the optical domain are constrained to stars hotter than B2. As most of the B and Be-star spectra in our sample show helium lines in only one ionization state (He I), we started to study many combinations of He I

line ratios and used only those which showed a less dependence on the helium abundance. Fixing $\log g$ values, we calculated synthetic line profiles for different temperatures from 15000 to 30000 K and helium number abundances He/H ratios from 0.001 to 0.3. Figures 3 and 4 shows several equivalent width ratios of He I lines against effective temperature and He/H abundance ratios obtained for $\log g = 3.0$ and 4.0. The analyses performed with neutral helium lines (He I $\lambda\lambda$ 4009, 4026, 4121, 4144, 4388, 4438, 4471 and 4922) show that only a few combinations of them (He I 4922/He I 4026, He I 4438/He I 4144, He I 4438/He I 4009, He I 4144/He I 4121) are less sensitive to the helium content (Figures 3 and 4). These less dependent ratios are characterized to be ratios of singlets and with oscillator strengths ratios near to unity. Triplets are discarded since they depend in a major degree on abundance as their statistical weights are higher than for singlet transitions. On

the other hand transitions with higher oscillator strength values produce profiles with deeper absorptions and more dependent on abundance. Once established the final photospheric parameters, we assume that the properties of the stellar core are not strongly modified by the rotation, which enables us to determine bolometric luminosities L , masses M and ages t through interpolation in the evolutionary tracks of non-rotating stars calculated by Schaller et al. (1992). In this procedure we used a similar geometrical construction proposed in Myakutin & Piskunov (1995) enclosing the desired solution in a plane (x, y) (where in this case x stands for T_{eff} and y for $\log g$) among two isochrones with ages τ_1 and τ_2 and two evolutionary tracks with masses m_1 and m_2 where the four vertices are given by the pairs (x_{11}, y_{11}) , (x_{12}, y_{12}) , (x_{21}, y_{21}) and (x_{22}, y_{22}) . The gravity values in the evolutionary tracks were calculated from the relation:

$$\log g = \log \frac{M}{M_{\odot}} - \log \frac{L}{L_{\odot}} + 4 \log T_{\text{eff}} - 10.6113 \quad (8)$$

which arises directly from the Stefan-Boltzmann law. In this system we seek for a solution pair (x, y) contained in a straight line that intercepts the tracks m_1 and m_2 in the coordinates (x_{1s}, y_{1s}) and (x_{2s}, y_{2s}) . This way we deals with a system of four equations to solve:

$$\frac{y_{12} - y_{11}}{x_{12} - x_{11}} = \frac{y_{1s} - y_{11}}{x_{1s} - x_{11}} \quad (9)$$

$$\frac{y_{22} - y_{21}}{x_{22} - x_{21}} = \frac{y_{2s} - y_{21}}{x_{2s} - x_{21}} \quad (10)$$

$$\frac{y_{1s} - y_{2s}}{x_{1s} - x_{2s}} = \frac{y_{1s} - y}{x_{1s} - x} \quad (11)$$

$$\frac{(y_{1s} - y_{11})^2 + (x_{1s} - x_{11})^2}{(y_{12} - y_{11})^2 + (x_{12} - x_{11})^2} = \frac{(y_{2s} - y_{21})^2 + (x_{2s} - x_{21})^2}{(y_{22} - y_{21})^2 + (x_{22} - x_{21})^2} \quad (12)$$

The fundamental parameters determined in this work are presented in Table 2. Columns 1, 2, 3 and 4 stands for the object's name (HD code), projected rotational velocity ($V\sin i$ in km.s^{-1}), effective temperature (T_{eff} in K) and superficial gravity ($\log g$ in dex) respectively. By interpolating in the Schaller's et al. (1992) theoretical evolutionary tracks (taking $Z = 0.02$) using the effective temperatures and gravities determined from the analysis of line spectra we obtain estimates of their logarithmic ages, bolometric luminosities $\log L/L_{\odot}$ and masses M/M_{\odot} , represented in columns 5, 6 and 7 of Table 2 respectively. The spectral types and luminosity classes presented in column 8 are taken from the SIMBAD database at the Centre de Données de Strasbourg (CDS). In column 9 it is provided the spectral classification based on the photospheric parameters evaluated in this work. In columns 10 and 11 we furnish estimates of deviations in temperature and gravity due to the effects of rapid rotation. These estimates were inferred, only in the case of Be stars, from the direct fitting of NLTE profiles affected by gravity darkening to the observed spectra. Column 12 shows the fractional age $\tau/\tau_{\text{M.S.}}$ only for Be stars. The positions of Be stars in the HR diagram are shown in Figure 5, whereas the evolutionary stages, corresponding to the entries in column 12, as a function of stellar masses are given in Figure 6, together with histograms of Be frequency counts for each specific mass range.

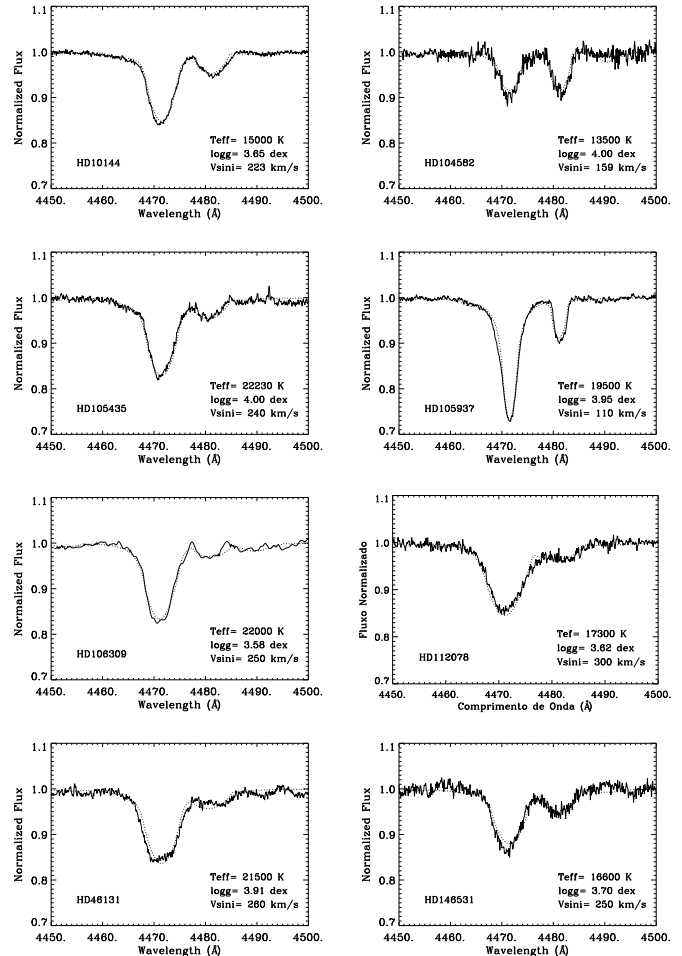


Figure 1. Sample of Be star spectra fitted with the Nelder & Mead algorithm (AMOEBA) in the spectral range of $\text{He I}\lambda 4471 \text{ Å}$ and $\text{Mg II}\lambda 4481 \text{ Å}$ line profiles.

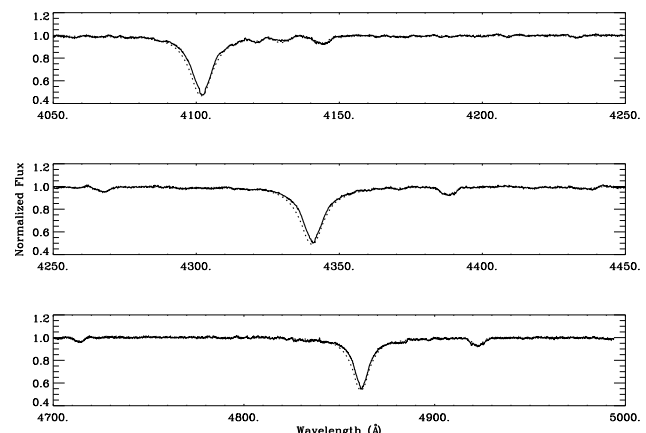


Figure 2. Comparison of model spectrum (dotted line) with the observed photospheric Balmer line profile (full lines) of the Be star Achernar. Upper panel: $\text{H}\beta$ line; middle panel: $\text{H}\gamma$ line; Lower panel: $\text{H}\delta$

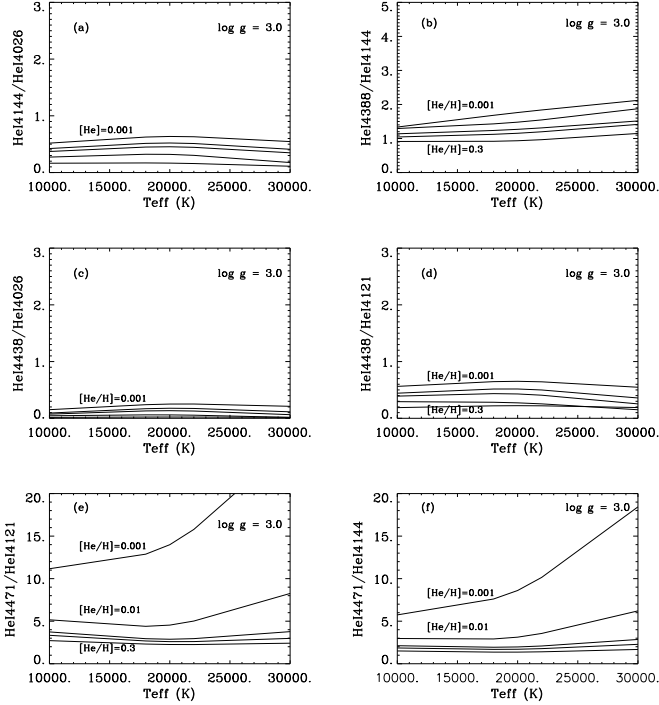


Figure 3. He I line equivalent width ratios as function of temperature and abundance, fixing $\log g = 3.0$ dex; (a) equivalent width ratios of He I 4144/He I 4026 and (b) He I 4388/He I 4144 do present less dependence with helium content; The same occurs in the case of ratios He I 4438/He I 4026 (c) and He I 4438/He I 4121 (d); In (e) we see the case of He I 4471/He I 4121 and (f) He I 4471/He I 4144, where the abundance dependence is higher.

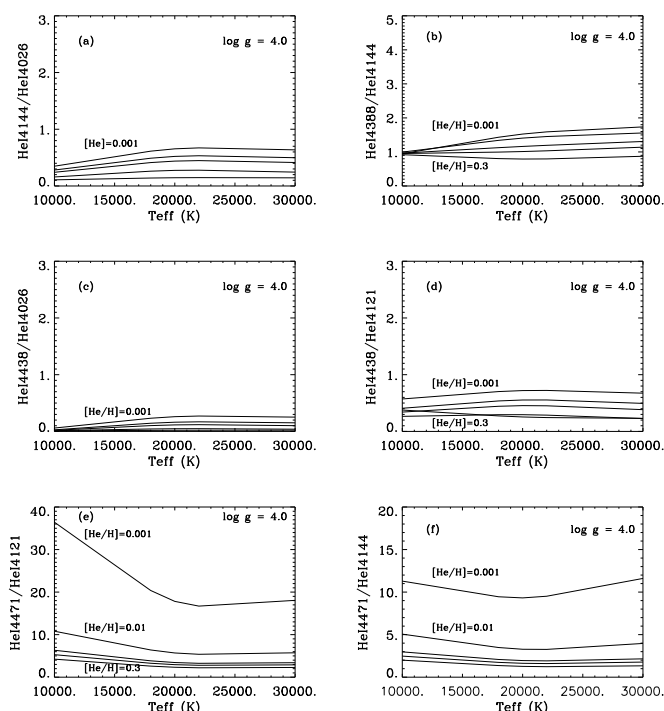


Figure 4. Same as figure 3, but for $\log g = 4.0$ dex.

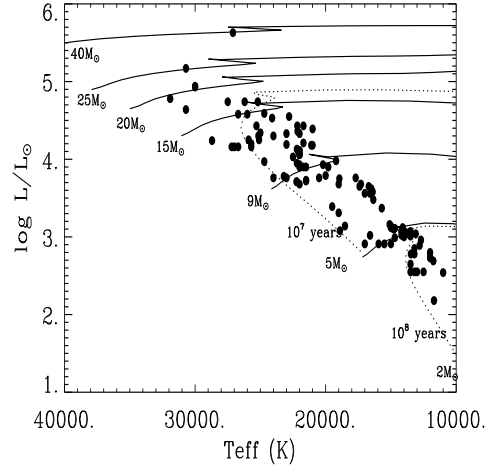


Figure 5. Location in the HR diagram ($\log L/L_{\odot}$, T_{eff}) of all observed Be stars neglecting the effects of high rotation. The evolutionary tracks (full lines) and isochrones (dashed lines) are from Schaller et al. (1992)

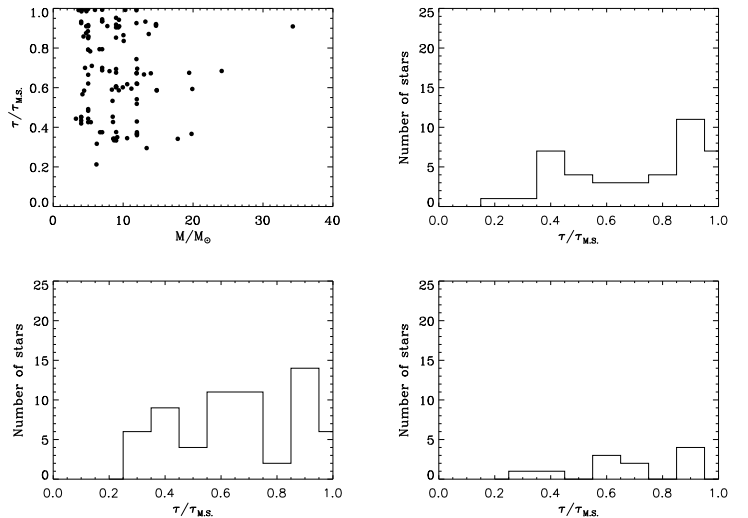


Figure 6. (up left) τ/τ_{MS} diagram as a function of mass for 114 field Be stars. (up right) Frequency counts of Be stars of low mass ($< 7M_{\odot}$) as a function of evolutionary stage in the mean sequence. (down left) Frequency counts of Be stars with intermediary mass (between 7 and $14M_{\odot}$) as a function of evolutionary stage. (down right) The same, but for higher masses (above $14M_{\odot}$).

2.2 Discussion

In this work we presented our first results of southern field B and Be star's photospheric parameters. The determination of effective temperatures (T_{eff}), superficial gravities ($\log g$) and projected rotation velocities ($V \sin i$) was achieved in three steps. In the first one we derived an initial value of $V \sin i$ from the average of values estimated by Fourier Transforms (FT) of all neutral helium line profiles in the wavelength domain from 4000 to 5000 Å. In the second step we derived T_{eff} and $\log g$ from the ionization equilibria of

He, O, N, Si and Balmer equivalent width fits, which delineate various minima in the Kiel diagram. In case of stars with strong emissions we adopted the background photospheric fitting procedure described in Chauville et al. (2001). We then adopted photometric indices in order to choose a well suitable region to apply spectral synthesis. In the last step we used a more accurate fitting procedure on conspicuous H and He lines with synthetic NLTE spectra (neglecting gravity darkening) to the observed data using the downhill simplex algorithm (AMOEBA) and limited the search to the best regions mentioned above. As our stellar sample are in average constrained to the solar vicinity, we can in principle consider all of them as possessing the same metallicity values (i.e. solar ones). Inspecting figure 6, in the $\tau/\tau_{\text{M.S.}} \times M/M_\odot$ diagram, we see clearly a tendency of occurrence of Be stars in the second half of the main sequence phase. Dividing this stellar sample in three subgroups, namely those with low mass ($M < 7M_\odot$), intermediate ($7M_\odot < M < 14M_\odot$), and higher masses ($M > 14M_\odot$), we get the histograms shown in the same figure. According to that we can have a “fast visual insight” on the dependence of the occurrence of the Be phenomenon with the stellar mass. For low massive stars, the Be phenomenon starts to occur even in earlier stages in the main sequence, but preferably in the second half of the main sequence, as they evolve more slowly and have time enough for that. As the stellar mass increases, it turns out to be more difficult to find Be stars in earlier stages, as they walk faster to the TAMS and this way it is more difficult to precise when the star started to display the phenomenon.

As a general result, without taking into account for rotational effects on the stellar spectra, B stars seem to display the Be phenomenon in the second half of the main sequence evolutionary phase. This result implies the existence of some evolutionary change that enables the appearance of the Be phenomenon during the MS lifetime and agree with those reported by many authors (McSwain & Gies 2005; Fabregat & Torrejón 2000; Meynet & Maeder 2002; Keller et al. 2001, Lyubimkov 1998). On the other hand, Zorec, Frémat & Cidale (2005) analysed a sample of 97 Be stars using models of rotating stars and showed that, when rotational effects take place, the Be phenomenon occurs elsewhere in the main sequence.

In order to constrain statistically the role of mass in the occurrence of the Be phenomenon, as well as to confirm the effects of gravity darkening in its appearance among B stars, it is important to analyse in the future a larger stellar sample.

ACKNOWLEDGMENTS

RSL and NVL warmly thanks and are in debt to Dr. J. Zorec for his advices as well as to Drs. Y. Frémat, J. Chauville, D. Ballereau, A.M. Hubert and M. Floquet for fruitful discussions. The authors are also grateful to an anonymous referee for valuable comments and suggestions which improved this work. This research was supported by FAPESP (Fundação de Amparo à Pesquisa do Estado de São Paulo) through grants no. 04/14256-8, 00/10029-6 and 1998/10138-8.

REFERENCES

- Carroll, J. A. 1933, MNRAS, 93, 478
- Chauville, J., Zorec, J., & Ballereau, D. et al. 2001, A&A, 378, 861
- Crampin, J., & Hoyle, F. 1960, MNRAS, 120, 33
- Fabregat J., & Torrejón J.M 2000, A&A, 357, 451
- Frémat, Y., Zorec, J., Hubert, A.M., Floquet, M. 2005, A&A, 440, 305
- Gray, D. F. 1992, in The observations and analysis of stellar atmospheres, ed. Cambridge Uni. Press, 368
- Hubeny, I. 1988, Computer Physics Comm. 52, 103
- Hubeny, I., Hummer, D.G., & Lanz, T. 1994, A&A, 282, 151
- Keller, S.C., Grebel, E.K., Miller, G.J., & Yoss, K.M., 2001, AJ, 122, 248
- Kurucz, R. L. 1992, CD-Rom 13, ATLAS 9 Stellar Atmosphere Programs and 2 km/s Grid (Cambridge: SAO)
- Levenhagen, R.S., Leister, N.V., Zorec, J., Janot-Pacheco, E., Hubert, A.M., Floquet, M. 2003, A&A, 400, 599
- Levenhagen, R.S., & Leister, N.V. 2004, AJ, 127, 1176
- Levenhagen, R.S. 2004, Ph.D. Thesis, IAG-USP
- Lyubimkov, L. S. 1998, Astronomy Reports, vol. 42, p. 52
- McSwain, M. V., Gies, D. R. 2005, ApJSS, 161, 118
- Maeder, A. 1999, A&A, 347, 185
- Maeder, A., Grebel, E.K., & Mermilliod, J.C 1999, A&A, 346, 459
- Meynet, G., Maeder, A. 2002, A&A, 390, 561
- Mermilliod, J. C. 1982, A&A, 109, 48
- Moujtahid, A., Zorec, J., Hubert, A. M. 1999, A&A, 349, 151
- Myakutin, V. I., Piskunov, A. Eh., 1995, AZh, 72, 358
- Nelder, J. A., & Mead, R. 1965, Computer Journal, vol. 7, 308
- Porter, J. M., Rivinius, Th. 2003, PASP, 115, 1153
- Schaller, G., Schaerer, D., Meynet, G., et al. 1992, A&AS, 96, 269
- Schild, R., Romanishin, W. 1976, ApJ, 204, 493
- Schmidt-Kaler, T. 1964, Bonn Verröff., 70, 1
- Slettebak, A. 1985, ApJS, 59, 769
- Townsend, R. H. D., Owocki, S. P., Howarth, I. D., 2004, MNRAS, 350, 189
- Vinicio, M. M. F., Zorec, J., Leister, N. V., Levenhagen, R. S. 2006, A&A, 446, 643
- von Zeipel, H. 1924a, MNRAS, 84, 665
- von Zeipel, H. 1924b, MNRAS, 84, 684
- Wade, R. A., Rucinski, S. M. 1985, A&A, 60, 471
- Zorec, J., Frémat, Y. & Cidale, L. 2005, A&A, 441, 235
- Zorec, J., & Briot, D. 1997, A&A, 318, 443

This paper has been typeset from a T_EX/ L^AT_EX file prepared
by the author.

Table 2: Photospheric parameters of target stars.

Object	$V \sin i$ (km s $^{-1}$)	T _{eff} (K)	log g(dex)	log Age(yr)	log L/L_{\odot}	M/M_{\odot}	Sp.T.(Simbad)	Sp.T.(this work)	ΔT_{eff} (K)	$\Delta \log g$ (dex)	$\tau/\tau_{M,S}$
HD 10144	223 ± 15	15000 ± 600	3.60 ± 0.10	7.99 ± 0.08	3.14 ± 0.10	4.9 ± 0.4	B3Vpe	B6Vpe	900	0.2	0.91
HD 14850	150 ± 20	13500 ± 550	3.60 ± 0.10	8.05 ± 0.06	3.01 ± 0.10	4.75 ± 0.10	B8Ve	B8Ve	350	0.1	0.99
HD 15371	10 ± 8	14700 ± 400	3.50 ± 0.10	7.97 ± 0.17	3.07 ± 0.20	5.0 ± 0.8	B5IV	B7IV			
HD 16582	12 ± 9	21500 ± 500	4.10 ± 0.10	7.26 ± 0.07	3.60 ± 0.10	7.9 ± 0.3	B2IV	B2/B3V			
HD 17891	70 ± 8	15150 ± 400	3.55 ± 0.10	7.97 ± 0.05	3.11 ± 0.10	5.0 ± 0.3	B9	B6V			
HD 20340	200 ± 18	18950 ± 450	3.65 ± 0.10	7.49 ± 0.05	3.75 ± 0.10	8.1 ± 0.7	B3V	B3Ve	900	0.2	0.68
HD 28248	30 ± 11	20000 ± 500	4.03 ± 0.10	7.34 ± 0.14	3.39 ± 0.08	7.00 ± 0.20	A1/A2V	B3V			
HD 29557	355 ± 22	19000 ± 450	4.00 ± 0.10	7.42 ± 0.09	3.31 ± 0.09	6.70 ± 0.10	B5IB/Iib	B3Ve	2000	0.3	0.38
HD 33453	290 ± 22	13700 ± 400	3.60 ± 0.15	7.95 ± 0.02	3.04 ± 0.10	5.00 ± 0.20	B8Vn	B8Vne	1500	0.3	0.79
HD 33599	200 ± 21	23200 ± 500	4.03 ± 0.10	7.12 ± 0.13	3.78 ± 0.10	9.2 ± 0.3	B5psb	B2Vpe	700	0.1	0.35
HD 35165	350 ± 23	21500 ± 500	3.77 ± 0.10	7.34 ± 0.10	3.90 ± 0.10	8.9 ± 0.3	B5IVnpe	B2Vnpe	1900	0.3	0.6
HD 35468	40 ± 12	21700 ± 500	4.00 ± 0.10	7.21 ± 0.11	3.65 ± 0.05	8.40 ± 0.10	B2III	B2V			
HD 36012	180 ± 13	21700 ± 500	3.52 ± 0.10	7.34 ± 0.02	4.21 ± 0.20	10 ± 1	B5Vne	B2Vne	700	0.2	0.99
HD 36861	55 ± 10	34000 ± 500	3.82 ± 0.10	6.59 ± 0.15	5.06 ± 0.20	25 ± 2	O8III	O8V			
HD 37023	50 ± 10	24200 ± 450	3.81 ± 0.15	7.13 ± 0.03	4.17 ± 0.20	11 ± 1	B0.5Vp	B1.5Vp			
HD 37490	170 ± 15	19000 ± 500	3.59 ± 0.10	7.64 ± 0.09	3.68 ± 0.10	7.0 ± 0.5	B3IIe	B3Ve	700	0.2	0.94
HD 37795	180 ± 15	14200 ± 400	3.50 ± 0.10	7.97 ± 0.12	3.07 ± 0.20	5.0 ± 0.5	B7IVe	B9Ve	1500	0.2	0.91
HD 43122	265 ± 18	25300 ± 600	3.63 ± 0.10	7.10 ± 0.09	4.4 ± 0.3	13 ± 2	B8	B1Ve	1200	0.05	0.67
HD 43285	237 ± 11	16600 ± 600	4.00 ± 0.10	7.74 ± 0.08	3.02 ± 0.10	5.38 ± 0.20	B6Ve	B6Ve	900	0.2	0.43
HD 43544	260 ± 22	21500 ± 500	3.91 ± 0.10	7.29 ± 0.09	3.72 ± 0.10	8.51 ± 0.10	B2/B3V	B2/B3Ve	1200	0.2	0.45
HD 43789	255 ± 19	15100 ± 400	3.70 ± 0.15	7.86 ± 0.05	3.16 ± 0.10	5.5 ± 0.3	B6V	B6/B7Ve	900	0.2	0.71
HD 44743	20 ± 7	24000 ± 500	3.43 ± 0.10	7.06 ± 0.04	4.70 ± 0.10	14.7 ± 0.3	B1II/III	B1.5IV			
HD 44996	38 ± 11	15200 ± 500	3.90 ± 0.10	7.85 ± 0.07	2.90 ± 0.15	5.00 ± 0.20	B4V	B6/B7V			
HD 45871	275 ± 15	20000 ± 500	3.72 ± 0.10	7.42 ± 0.08	3.79 ± 0.10	8.39 ± 0.20	B4Vnpe	B3Ve	1500	0.3	0.59
HD 46131	275 ± 18	19500 ± 600	4.05 ± 0.15	7.34 ± 0.06	3.39 ± 0.10	7.00 ± 0.20	B4V	B3Ve	1500	0.3	0.38
HD 46380	293 ± 30	21100 ± 650	3.50 ± 0.10	7.35 ± 0.05	4.18 ± 0.10	10.1 ± 0.9	B2Vne	B2/B3IVnpe	1600	0.3	0.84
HD 47839	70 ± 10	25200 ± 500	3.50 ± 0.10	7.06 ± 0.06	4.74 ± 0.10	14.7 ± 0.3	O7Ve	B1Ve	400	0.1	0.92
HD 48099	115 ± 12	30700 ± 700	3.53 ± 0.10	6.75 ± 0.04	5.17 ± 0.10	24 ± 1	O6e	B0Ve	100	0.05	0.68
HD 48282	188 ± 18	18520 ± 550	4.10 ± 0.15	7.35 ± 0.20	3.14 ± 0.10	6.2 ± 0.7	B3III	B3Ve	1200	0.2	0.32
HD 49131	135 ± 15	20000 ± 500	3.60 ± 0.10	7.42 ± 0.15	4.00 ± 0.20	9 ± 1	B2III	B3V			
HD 49319	245 ± 18	21000 ± 500	3.40 ± 0.15	7.20 ± 0.05	4.39 ± 0.20	12 ± 1	B6Vnne	B2/B3IVnpe	1400	0.3	0.93
HD 49330	200 ± 10	27200 ± 600	4.00 ± 0.10	6.91 ± 0.20	4.16 ± 0.10	11.9 ± 0.4	B0:nnpe	B1Vnpe	300	0.05	0.36
HD 49336	220 ± 15	16400 ± 500	3.59 ± 0.10	7.61 ± 0.20	3.58 ± 0.10	7.00 ± 0.10	B4Vne	B6Vne	1100	0.2	0.79
HD 50013	210 ± 20	24100 ± 500	3.58 ± 0.10	7.05 ± 0.02	4.53 ± 0.05	14 ± 1	B1.5IVe	B1.5Ve	600	0.1	0.67
HD 50209	173 ± 15	12500 ± 450	4.00 ± 0.15	8.03 ± 0.20	2.55 ± 0.30	4 ± 0.9	B9Ve	B9Ve	200	0.05	0.45
HD 50696	281 ± 18	21700 ± 600	3.50 ± 0.15	7.20 ± 0.10	4.43 ± 0.25	12 ± 1	B1:V:nne	B2Vnne	1400	0.3	1
HD 50737	230 ± 20	22200 ± 600	4.00 ± 0.15	7.17 ± 0.10	3.71 ± 0.10	8.7 ± 0.3	B2Vnne	B2Vnne	800	0.2	0.33
HD 50850	310 ± 26	18900 ± 600	4.20 ± 0.10	7.02 ± 0.20	3.08 ± 0.09	6.18 ± 0.10	B3:Vnne	B3:Vnne	1600	0.3	0.21
HD 51309	28 ± 9	18900 ± 500	3.53 ± 0.15	7.41 ± 0.08	3.98 ± 0.20	9 ± 1	B3Ib/II	B3V			
HD 52159	110 ± 17	17700 ± 550	3.50 ± 0.15	7.56 ± 0.08	3.76 ± 0.20	7.7 ± 0.8	B5Vne	B3Vne	700	0.1	0.91
HD 52244	210 ± 22	22170 ± 550	3.50 ± 0.10	7.20 ± 0.04	4.43 ± 0.15	12 ± 1	B2:III:nnpe	B2IVnpe	800	0.2	0.99
HD 55606	335 ± 20	28700 ± 550	4.10 ± 0.10	6.68 ± 0.25	4.24 ± 0.12	14 ± 1	B1:V:nnpe	B0.5Vnnpe	100	0.05	0.3
HD 58715	230 ± 20	13100 ± 400	3.61 ± 0.10	7.95 ± 0.07	3.04 ± 0.10	5.00 ± 0.10	B8Ve	B8Ve	700	0.1	0.79
HD 59868	200 ± 18	17000 ± 500	3.82 ± 0.10	7.70 ± 0.06	3.25 ± 0.30	6.1 ± 1	B8IV/V	B3V			
HD 63150	260 ± 15	25150 ± 450	3.75 ± 0.15	7.12 ± 0.10	4.30 ± 0.20	12 ± 1	B1.5Vnne	B1Ve	1100	0.05	0.62
HD 67698	90 ± 11	17400 ± 500	3.55 ± 0.10	7.63 ± 0.14	3.65 ± 0.10	7 ± 1	B3III/IV	B3Ve	700	0.1	1
HD 70461	266 ± 15	15940 ± 550	3.95 ± 0.10	7.79 ± 0.10	2.91 ± 0.10	5.0 ± 0.5	B5	B6Ve	900	0.2	0.48
HD 74280	120 ± 15	18000 ± 500	4.00 ± 0.10	7.52 ± 0.12	3.18 ± 0.08	6.2 ± 0.3	B3V	B3V			
HD 79447	13 ± 8	18900 ± 500	3.50 ± 0.10	7.43 ± 0.03	3.94 ± 0.08	8.78 ± 0.3	B3III	B3V			
HD 90177	10 ± 5	14100 ± 400	3.58 ± 0.10	7.91 ± 0.03	3.1 ± 0.3	5.29 ± 1	B2evar	B7Ve	300	0.05	0.78
HD 97991	150 ± 10	21000 ± 400	4.01 ± 0.10	7.45 ± 0.10	3.56 ± 0.10	7.80 ± 0.10	B2/B3V	B2/B3V			
HD 100546	85 ± 20	11750 ± 600	3.50 ± 0.10	8.21 ± 0.10	2.69 ± 0.25	4 ± 1	B9Vne	B9Vne	100	0.05	0.93
HD 100889	180 ± 18	12100 ± 400	4.00 ± 0.10	8.24 ± 0.14	2.26 ± 0.10	3.41 ± 0.12	B9.5Vn	B9.5V			
HD 104582	159 ± 16	13500 ± 500	4.00 ± 0.15	8.03 ± 0.10	2.55 ± 0.17	4.0 ± 0.8	B8/B9II/III	B8/B9Ve	200	0.05	0.45
HD 105435	240 ± 32	22230 ± 650	4.00 ± 0.10	7.17 ± 0.15	3.71 ± 0.10	8.72 ± 0.3	B2IVnpe	B2Vne	900	0.2	0.34
HD 105521	160 ± 18	19200 ± 550	3.50 ± 0.10	7.41 ± 0.10	3.98 ± 0.25	8.98 ± 1	B3IVe	B3IVe	500	0.2	0.85
HD 105937	110 ± 20	19500 ± 600	3.95 ± 0.10	7.44 ± 0.04	3.45 ± 0.07	7.03 ± 0.17	B3V	B3V			
HD 106309	250 ± 28	22000 ± 500	3.58 ± 0.10	7.42 ± 0.10	4.06 ± 0.07	9 ± 1	B2IV:ne	B2IVnpe	1200	0.2	0.9
HD 106793	277 ± 20	13880 ± 450	3.53 ± 0.15	7.96 ± 0.10	3.06 ± 0.10	5.0 ± 0.5	B8/B9II/IIIe	B8/B9IVe	1400	0.3	0.85
HD 110432	400 ± 30	27100 ± 650	3.00 ± 0.10	6.66 ± 0.04	5.63 ± 0.21	34.26 ± 5	B2pe	B0.5IVpe	1600	0.05	0.91
HD 110699	150 ± 15	15000 ± 500	3.62 ± 0.10	7.98 ± 0.02	3.12 ± 0.20	5.0 ± 0.4	B9.5:V:n	B6Vne	400	0.05	0.92
HD 112078	300 ± 20	17300 ± 450	3.62 ± 0.10	7.64 ± 0.03	3.68 ± 0.03	7.00 ± 0.13	B4Vne	B3Vne	1800	0.36	0.94
HD 112091	230 ± 20	16500 ± 550	3.50 ± 0.10	7.63 ± 0.10	3.62 ± 0.16	7.0 ± 0.7	B5Vne	B5Vne	1200	0.25	0.95
HD 112107	200 ± 19	12000 ± 400	3.58 ± 0.10	8.21 ± 0.15	2.74 ± 0.14	4.04 ± 0.18	B9.5Vn	B9.5Vne	400	0.05	0.99
HD 112512	199 ± 20	14180 ± 400	3.69 ± 0.15	7.93 ± 0.06	3.02 ± 0.15	5.0 ± 0.5	B7III	B7Ve	600	0.1	0.67
HD 113120	320 ± 20	22800 ± 500	3.42 ± 0.10	7.11 ± 0.05	4.55 ± 0.06	14 ± 1	B1.5IIIne	B2IVnne	1700	0.2	0.87
HD 118094	239 ± 30	13500 ± 550	3.90 ± 0.15	8.06 ± 0.04	2.65 ± 0.08	4.18 ± 0.20	B8Vn...	B8Vne	600	0.1	0.57
HD 119423	180 ± 15	17000 ± 600	3.95 ± 0.15	7.79 ± 0.13	2.91 ± 0.20	5.0 ± 0.4	B4:Vne	B3Vne	700	0.2	0.43
HD 119682	200 ± 20	31910 ± 550	4.00 ± 0.10	6.59 ± 0.10	4.78 ± 0.10	20 ± 1	O+...	B0Ve	100	0.05	0.37
HD 120324	125 ± 16	22500 ± 550	3.75 ± 0.15	7.28 ± 0.25	4.03 ± 0.11	9.95 ± 0.2	B2Vnpe	B2Vnpe	700	0.1	0.6
HD 120991	130 ± 16	22000 ± 500	3.57 ± 0.10	7.42 ± 0.02	4.06 ± 0.13	8.9 ± 0.5	B2IIIe	B2Ve	500	0.1	0.92

Table 2: Continued.

Object	$V \sin i$ (km s $^{-1}$)	T _{eff} (K)	log g(dex)	log Age(yr)	log L/L_{\odot}	M/M_{\odot}	Sp.T.(Simbad)	Sp.T.(this work)	ΔT_{eff} (K)	$\Delta \log g$ (dex)	$\tau/\tau_{\text{M.S.}}$
HD 124639	237 ± 30	12700 ± 600	3.50 ± 0.10	8.05 ± 0.09	2.96 ± 0.14	4.7 ± 0.3	B8Ve	B9IVe	900	0.2	0.91
HD 125924	75 ± 12	21000 ± 400	4.10 ± 0.15	7.10 ± 0.15	3.77 ± 0.16	8.90 ± 0.10	B2IV	B2IV			
HD 126527	235 ± 25	13200 ± 450	3.67 ± 0.10	8.05 ± 0.08	2.85 ± 0.17	4.5 ± 0.3	B8V	B9Ve	600	0.1	0.7
HD 126986	70 ± 15	12000 ± 400	3.54 ± 0.10	8.14 ± 0.11	2.80 ± 0.17	4.3 ± 0.4	B9.5Vnn...	B9IVne	200	0.05	0.86
HD 127112	115 ± 20	14000 ± 500	3.63 ± 0.15	8.06 ± 0.20	3.00 ± 0.20	4.7 ± 0.3	B7III	B8Ve	300	0.05	0.88
HD 127208	150 ± 20	12000 ± 500	3.55 ± 0.10	8.22 ± 0.15	2.73 ± 0.10	4.00 ± 0.18	B8Ve	B9IVe	200	0.05	0.99
HD 127381	80 ± 14	23000 ± 550	4.02 ± 0.10	7.13 ± 0.13	3.76 ± 0.06	9 ± 0.5	B2III	B1/B2V			
HD 127972	310 ± 20	20500 ± 600	3.80 ± 0.10	7.36 ± 0.1	3.76 ± 0.16	8.5 ± 0.9	B1.5Vne	B2Ve	1500	0.3	0.53
HD 129956	80 ± 15	11500 ± 400	3.61 ± 0.10	8.19 ± 0.03	2.66 ± 0.06	4 ± 0.13	B9.5V	B9.5V			
HD 130437	335 ± 25	24700 ± 500	3.52 ± 0.15	7.15 ± 0.02	4.59 ± 0.09	13.2 ± 0.7	O+...	B1Ve	1700	0.2	0.93
HD 130534	100 ± 20	14700 ± 400	3.55 ± 0.15	7.97 ± 0.13	3.11 ± 0.20	5 ± 1	B3III	B7Ve	200	0.05	1
HD 131168	185 ± 22	22000 ± 500	3.70 ± 0.10	7.34 ± 0.09	3.90 ± 0.11	8.9 ± 0.4	B3Ve	B2Ve	800	0.1	0.6
HD 132947	150 ± 20	13000 ± 500	4.05 ± 0.10	8.06 ± 0.08	2.35 ± 0.23	3.7 ± 0.4	A0	B9V			
HD 134401	375 ± 25	22200 ± 500	3.77 ± 0.10	7.32 ± 0.12	3.95 ± 0.11	9.4 ± 0.4	B2Vne	B2Vne	2000	0.35	0.59
HD 134481	146 ± 19	11700 ± 500	4.00 ± 0.10	8.29 ± 0.08	2.18 ± 0.20	3.25 ± 0.10	B9.5Vne	B9.5Vne	100	0.05	0.44
HD 134671	250 ± 19	14700 ± 400	3.81 ± 0.15	7.90 ± 0.05	2.99 ± 0.09	5 ± 0.2	B7II	B7Ve	800	0.2	0.62
HD 135734	280 ± 20	13470 ± 500	3.80 ± 0.10	8.05 ± 0.05	2.78 ± 0.10	4.42 ± 0.20	B8Ve	B8Ve	900	0.2	0.59
HD 136968	207 ± 19	16350 ± 400	3.57 ± 0.10	7.7 ± 0.15	3.48 ± 0.10	7 ± 1	B5Vne	B5Vne	1000	0.2	0.79
HD 137387	250 ± 21	21500 ± 500	3.90 ± 0.10	7.29 ± 0.18	3.73 ± 0.15	8.6 ± 0.9	B1npe	B2Vnpe	1100	0.2	0.43
HD 137518	300 ± 25	25900 ± 400	3.82 ± 0.15	7.07 ± 0.17	4.25 ± 0.24	12 ± 1	B1/B2III:n...	B1Vne	1000	0.1	0.54
HD 142237	345 ± 27	26000 ± 500	3.63 ± 0.10	6.98 ± 0.14	4.58 ± 0.10	14.8 ± 0.4	B2Vne	B1Vne	300	0.1	0.59
HD 142349	250 ± 25	16600 ± 550	3.70 ± 0.10	7.58 ± 0.08	3.56 ± 0.08	7.00 ± 0.20	B5IV	B5Ve	700	0.2	0.7
HD 143545	370 ± 30	23000 ± 550	3.70 ± 0.15	7.19 ± 0.23	4.19 ± 0.20	11.18 ± 0.20	B1/B2ne	B1/B2Vne	2100	0.3	0.6
HD 143578	164 ± 16	13500 ± 400	3.55 ± 0.10	7.96 ± 0.05	3.07 ± 0.10	5.0 ± 0.5	B8IV/V	B8IV/V	400	0.1	0.86
HD 143700	230 ± 20	23000 ± 500	3.60 ± 0.10	7.15 ± 0.36	4.33 ± 0.20	12 ± 1	B2/B3III:n:e	B1/B2Vne	1000	0.1	0.67
HD 144555	275 ± 23	24000 ± 450	3.73 ± 0.10	7.12 ± 0.18	4.30 ± 0.08	12 ± 1	B2IB:n:e	B1Vne	1100	0.2	0.62
HD 146531	260 ± 25	17000 ± 500	3.67 ± 0.10	7.58 ± 0.21	3.56 ± 0.10	7.00 ± 0.16	B6III	B3Ve	1300	0.3	0.69
HD 149757	340 ± 20	27000 ± 650	4.00 ± 0.10	6.91 ± 0.20	4.16 ± 0.10	12 ± 1	O9V	B0.5Ve	200	0.1	0.37
HD 150193	65 ± 15	11000 ± 400	3.58 ± 0.10	8.37 ± 0.15	2.54 ± 0.08	3.62 ± 0.10	A1Ve	B9.5Ve	300	0.05	0.99
HD 150288	250 ± 23	22000 ± 450	3.58 ± 0.10	7.42 ± 0.09	4.06 ± 0.12	8.9 ± 0.5	B3V	B2Ve	1200	0.2	0.95
HD 150422	270 ± 26	25100 ± 400	3.83 ± 0.10	7.07 ± 0.03	4.25 ± 0.08	11.9 ± 0.3	B1/B2ne	B1Vne	1100	0.1	0.52
HD 151113	180 ± 20	21700 ± 600	3.71 ± 0.10	7.34 ± 0.11	3.90 ± 0.10	8.9 ± 0.5	B5II/III	B2Ve	800	0.2	0.61
HD 152060	105 ± 12	22000 ± 500	3.64 ± 0.15	7.15 ± 0.18	4.33 ± 0.15	11.9 ± 0.4	B1III	B2Ve	700	0.1	0.67
HD 152478	295 ± 22	19800 ± 500	3.75 ± 0.10	7.34 ± 0.09	3.90 ± 0.08	8.99 ± 0.2	B3Vnpe	B3Vnpe	1600	0.3	0.61
HD 152979	190 ± 20	21000 ± 500	3.51 ± 0.10	7.35 ± 0.08	4.18 ± 0.08	10.04 ± 0.10	B2IV	B2IV	900	0.2	0.87
HD 153199	190 ± 19	20200 ± 500	3.65 ± 0.10	7.37 ± 0.09	3.93 ± 0.10	8.9 ± 0.5	B3II/III	B2/B3Ve	900	0.2	0.69
HD 154154	290 ± 25	25000 ± 500	3.65 ± 0.15	7.15 ± 0.03	4.34 ± 0.10	12.01 ± 0.20	B2Vnne	B1Vnne	1400	0.05	0.7
HD 155851	335 ± 30	30000 ± 700	3.65 ± 0.10	6.81 ± 0.14	4.93 ± 0.15	19.89 ± 0.20	B0Vn	B0Vn	1000	0.1	0.59
HD 156325	180 ± 24	15700 ± 500	3.57 ± 0.15	7.84 ± 0.08	3.37 ± 0.20	6 ± 1	B5Vne	B6Vne	700	0.1	0.99
HD 156702	265 ± 26	24700 ± 500	4.01 ± 0.10	7.03 ± 0.12	3.97 ± 0.10	10.57 ± 0.20	B5	B1Ve	800	0.1	0.35
HD 158427	270 ± 25	22150 ± 550	3.55 ± 0.10	7.17 ± 0.10	4.36 ± 0.10	11.90 ± 0.20	B2Vne	B2Vne	1400	0.2	0.74
HD 159489	170 ± 18	25700 ± 500	4.04 ± 0.10	6.91 ± 0.14	4.16 ± 0.10	11.97 ± 0.20	B3IV	B1Ve	700	0.05	0.37
HD 160202	220 ± 21	16700 ± 500	3.55 ± 0.10	7.63 ± 0.17	3.65 ± 0.10	7.00 ± 0.10	B7Ve	B5Ve	1200	0.2	0.99
HD 161774	100 ± 10	13200 ± 500	3.63 ± 0.15	8.22 ± 0.10	2.78 ± 0.10	4.00 ± 0.20	B5V:nn:e	B8Vnne	200	0.05	0.93
HD 164284	220 ± 20	22200 ± 400	3.60 ± 0.15	7.39 ± 0.16	4.13 ± 0.08	9 ± 1	B2Ve	B2Ve	1000	0.2	0.91
HD 164816	95 ± 15	20000 ± 500	3.53 ± 0.10	7.44 ± 0.08	4.01 ± 0.05	8.87 ± 0.60	O+...	B3Ve	500	0.1	0.81
HD 164906	255 ± 20	30700 ± 550	3.95 ± 0.15	6.67 ± 0.20	4.64 ± 0.15	18 ± 1	B0Ve	B0Ve	100	0.05	0.34
HD 164947	120 ± 20	23000 ± 500	4 ± 0.10	7.13 ± 0.20	3.76 ± 0.15	9.00 ± 0.20	B2V:n:e	B1/B2Vne	700	0.1	0.38
HD 165052	125 ± 22	37500 ± 550	4.10 ± 0.10	5.97 ± 0.04	4.9 ± 0.3	25 ± 3	O6.5V	O6.5V			
HD 166566	50 ± 10	22000 ± 500	3.60 ± 0.10	7.40 ± 0.09	4.11 ± 0.10	9.3 ± 0.3	B1II:ne	B2Ve	400	0.1	0.9
HD 170235	170 ± 18	26200 ± 500	3.50 ± 0.10	7.06 ± 0.12	4.74 ± 0.10	15 ± 1	B2Vnne	B1Vnne	100	0.05	0.92
HD 170835	260 ± 23	22000 ± 500	3.69 ± 0.10	7.24 ± 0.09	4.11 ± 0.10	10.6 ± 0.3	B5IV	B2Ve	1400	0.2	0.62
HD 171054	40 ± 10	22000 ± 550	4.00 ± 0.15	7.18 ± 0.09	3.68 ± 0.10	8.6 ± 0.3	B2II	B2Ve	600	0.1	0.34
HD 171219	190 ± 25	13500 ± 500	3.80 ± 0.15	8.05 ± 0.11	2.78 ± 0.20	4.4 ± 0.3	B8	B8V			
HD 172256	310 ± 20	24000 ± 500	4.02 ± 0.10	7.13 ± 0.18	3.76 ± 0.10	9.0 ± 0.5	B5II	B1Ve	1200	0.2	0.3
HD 173948	130 ± 10	22000 ± 500	3.65 ± 0.10	7.37 ± 0.05	3.93 ± 0.10	8.9 ± 0.5	B2II-IIIe	B2Ve	700	0.1	0.68
HD 174705	210 ± 20	22150 ± 400	3.6 ± 0.10	7.40 ± 0.10	4.12 ± 0.10	9.4 ± 0.3	B2Vne	B2Vne	900	0.1	0.94
HD 179253	120 ± 13	14800 ± 500	3.62 ± 0.10	7.99 ± 0.06	3.10 ± 0.10	5.00 ± 0.10	B5V	B7Ve	300	0.1	0.89
HD 183914	220 ± 16	13200 ± 600	4 ± 0.15	8.03 ± 0.35	2.55 ± 0.15	4.0 ± 0.8	B8Ve	B8Ve	100	0.05	0.43
HD 184279	200 ± 22	30400 ± 600	3.90 ± 0.10	6.86 ± 0.07	4.49 ± 0.10	15 ± 1	B0.5IV	B0V			
HD 185037	280 ± 20	13000 ± 500	4.00 ± 0.10	8.03 ± 0.05	2.55 ± 0.15	4.0 ± 0.6	B8Vne	B8Vne	700	0.2	0.42
HD 198001	90 ± 10	11200 ± 400	4.01 ± 0.10	8.34 ± 0.14	2.07 ± 0.10	3.03 ± 0.10	A1.5V	B9.5V			
HD 205637	242 ± 21	18850 ± 400	3.95 ± 0.10	7.44 ± 0.05	3.44 ± 0.10	7.0 ± 0.5	B3V:p	B3V			
HD 208886	200 ± 20	15000 ± 450	4.01 ± 0.10	7.79 ± 0.09	2.91 ± 0.20	5.0 ± 0.5	B5III	B7Ve	400	0.1	0.49
HD 217891	90 ± 15	15500 ± 600	4.00 ± 0.10	7.79 ± 0.09	2.91 ± 0.16	5.0 ± 0.5	B6Ve	B6Ve	200	0.1	0.44
HD 224686	300 ± 20	13000 ± 500	3.90 ± 0.10	8.09 ± 0.09	2.59 ± 0.10	4.00 ± 0.20	B9IV	B8V			
HD 316341	120 ± 15	30000 ± 500	3.54 ± 0.10	6.85 ± 0.55	4.94 ± 0.20	19 ± 2	O+...	B0Ve	200	0.1	0.68
HD 316587	190 ± 15	25700 ± 500	3.90 ± 0.10	7 ± 0.15	4.20 ± 0.10	11.9 ± 0.6	B1V:n:e...	B1Vne	400	0.05	0.43
HD 322422	170 ± 15	26700 ± 550	3.65 ± 0.15	6.98 ± 0.21	4.58 ± 0.15	14.8 ± 0.3	B0.5IIe	B1Ve	200	0.05	0.59
HD 330950	60 ± 10	26700 ± 500	4.00 ± 0.10	6.91 ± 0.21	4.16 ± 0.15	11.9 ± 0.3	O+...	B1Ve	100	0.05	0.38